Journal of Applied Geophysics 68 (2009) 231–242

Contents lists available at ScienceDirect

Journal of Applied Geophysics

journal homepage: www.elsevier.com/locate/jappgeo

Inversion of teleseismic receiver function and magnetotelluric sounding to determine basement depth in the Paraná Basin, SE Brazil

Iván Zevallos [a], Marcelo Assumpção [a,*], Antonio L. Padilha [b]

[a] IAG-USP, Department of Geophysics, Institute of Astronomy, Geophysics and Atmospheric Sciences, São Paulo University, 05508-090, Brazil
[b] INPE, São José dos Campos - Brazil

ARTICLE INFO

Article history:
Received 5 June 2007
Accepted 11 November 2008

Keywords:
Receiver function
Magnetotellurics
Joint inversion
Flood basalts
Sedimentary basin
Genetic algorithm
Low-velocity zone

ABSTRACT

Flood basalts in the Paraná Basin make exploration of the deeper sedimentary sequence more difficult with seismic reflection methods. We present a new method to obtain information about sub-basalt layers by joint inversion of high-frequency Receiver Functions (RF) and Magnetotelluric (MT) data. Using genetic algorithm, which is more flexible to incorporate data variance in the objective function, we obtain 1D models of the main layers of the basin beneath three seismographic stations. We show that the joint inversion produces more stable models than inversion of RF or MT data alone. Thicknesses of the basalt layer were estimated at 1 km, and basement depth were found to range from 3.8 to 4.3 km, roughly consistent with expected values based on the sparse regional borehole data. Deep earthquakes in the nearby Nazca plate subduction zone are a good source of high frequency P-waves making the joint RF + MT inversion a promising method to study shallow intracratonic basins in Brazil, especially where the sedimentary structure can be represented by 1D models.

1. Introduction

Imaging sub-basalt layers by conventional seismic reflection methods can be a difficult problem in many areas (e.g., Moritz and White, 2001). Seismic surveys in the Paraná Basin in the 1980's could not always find the crystalline basement very clearly (Rosa et al., 1982; Souza, 1982). The high seismic velocity of the flood basalts (produced during continental breakup) create a major obstacle to imaging the lower seismic velocity sedimentary structures which underlie them (Moritz and White, 2001). The large acoustic impedance contrast (reflectivity coefficient) between the shallow weathered basalts and fresh volcanic rocks and between these and the sedimentary layers, rebound and scatter much of the incident seismic energy. Multiple reflections in the basalt layer often obscure the weak signals from the deeper interfaces and interference from interbedded units within the basalt act as a low-pass filter to the seismic waves (Ziolkowski and Fokkema, 1986; Souza, 1982). For these reasons, magnetotelluric soundings were used for a regional mapping of basement depths in the Paraná Basin (Stanley et al., 1985). Some alternatives have been proposed to improve the seismic response from basalt-covered areas, such as wide-angle data (Jarchow et al., 1994) and low-frequency reflection data (Souza, 1982; Ziolkowski et al., 2003). In our study we analyse data from distant earthquakes (teleseismic receiver functions) together with magnetotelluric soundings to investigate the main layers of the basalt covered intracratonic Paraná Basin and determine the basement depth.

Seismological methods have been extensively developed to extract information about the receiver structure beneath a seismic station from the records of distant earthquakes, called Receiver Function (RF) method (e.g., Langston, 1979; Owens et al., 1984; Wilson and Aster, 2003), and have been successfully used for deep crustal studies worldwide (e.g., Zandt and Ammon, 1995). Crustal studies in the Paraná Basin using RF (Assumpção et al., 2002; França & Assumpção, 2003; An and Assumpção, 2004a) show a series of shallow reverberations and conversions due to the sedimentary pack beneath the station. For deep crustal studies with RF, frequencies lower than about 1 Hz are commonly used. Much higher frequencies are necessary to study shallow layers. The Paraná Basin is conveniently located near the Nazca plate subduction zone, where the high frequency P waves from intermediate and deep earthquakes are not much attenuated since the propagation path avoids the asthenospheric wedge above the subduction zone, and the asthenosphere beneath the South American stable platform is not much developed.

Basement depth in the Paraná Basin has not been mapped in detail as relatively few oil exploration wells have been drilled deep enough (Fig. 1). Most wells drilled for ground water do not reach the crystalline basement, making isopack maps only useful at large regional scales. More accurate knowledge of basement depth will be necessary as ground water management is expected to become increasingly more important. Here we present the simultaneous inversion of RF and MT soundings to obtain 1D models of the main

* Corresponding author. IAG-USP, Rua do Matão 1226, Cidade Universitária, São Paulo, SP 05508-090, Brazil. Fax: +55 11 3091 5034.
E-mail addresses: ivanzev@gmail.com (I. Zevallos), marcelo@iag.usp.br (M. Assumpção), padilha@dge.inpe.br (A.L. Padilha).

0926-9851/$ – see front matter © 2008 Elsevier B.V. All rights reserved.
doi:10.1016/j.jappgeo.2008.11.002

features of the sedimentary pack and basement depth. This is based on the assumption that the main interfaces, such as basalt/sediment and sediment/basement, should have large contrasts in both seismic velocity and resistivity. Although single RF and MT inversions can be non-unique, we show that the joint inversion of both datasets substantially reduces the scatter of the possible models and makes this method a promising tool to investigate intracratonic basins where the generally small dip of the sedimentary layers render 1D models a useful approximation.

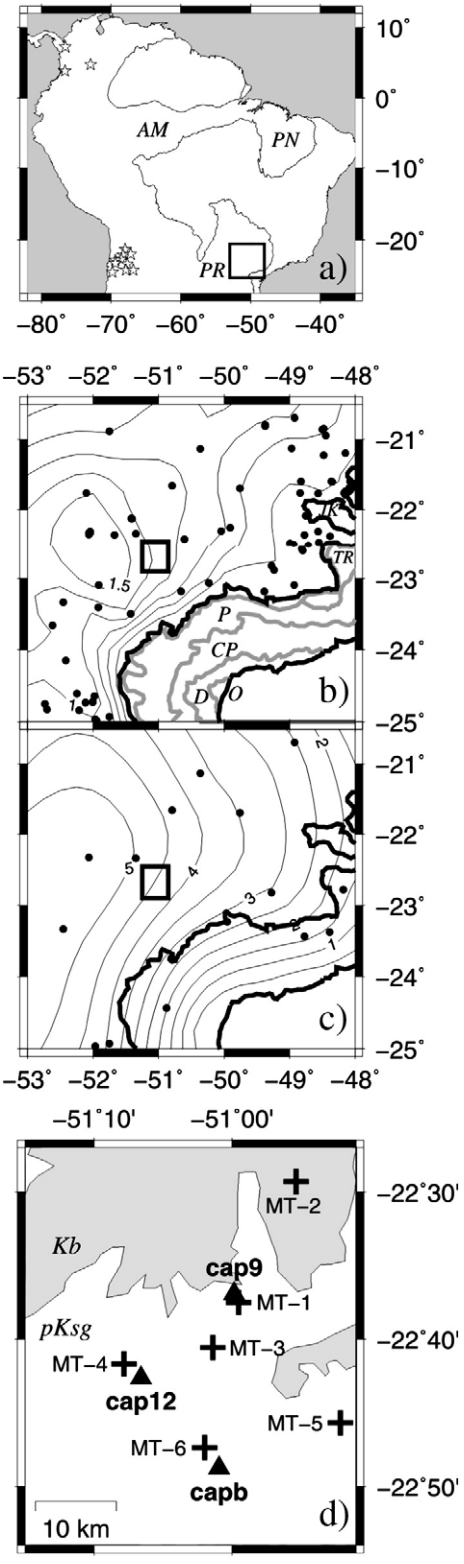

The basement beneath the Paraná Basin is formed by Neoproterozoic/Early Paleozoic igneous and metamorphic rocks of the Gondwana amalgamation in the Pan-African/Brasiliano orogen. The main sedimentary sequences of the Basin are exposed to the SE of our study area (Fig. 1b) and have an expected total thickness between 4 and 5 km (Fig. 1c). According to Milani et al. (1994), Milani and Ramos (1998) and Milani (2004), the first subsidence of the Basin occurred in the Neo-Ordovician (~440 Ma) and continental to marine glacial sediments, called Rio Ivaí Supersequence, were deposited which are probably less than 100 m thick beneath our study area (Milani and Ramos, 1998). After uplift and erosion, a second subsidence phase in the Devonian (Paraná Supersequence) caused deposition of about 500 m of fluvial to marine sediments of the Furnas and Ponta Grossa Formations. Another major unconformity separated this Devonian sequence from the next Supersequence, called Gondwana-I, deposited from the Neo-Carboniferous to Permian, ranging from glacial marine to continental eolic sediments, reaching more than 2 km beneath our study area. In this part of the Paraná Basin, the next subsidence phase, called Gondwana-III, started in Neo-Jurassic with the Botucatu Formation (desert sands forming the present Guarany Aquifer, probably only about 0.5 km thick) followed by the Eo-Cretaceous continental flood basalts (137–127 Ma), about 1.0 to 1.3 km thick (Fig. 1b). Basalt rocks (or basalt-derived soils) are the main surface exposure in our area (Fig. 1d). The last sedimentary sequence is the Neo-Cretaceous sandstone (Adamantina Formation of the Bauru Group) which is seen as a thin cap in the northern part of Fig. 1d.

Three seismic stations (*capb*, *cap12*, and *cap09*; Fig. 1d) were operated in 1994–1995 as part of the BLSP project (Brazilian Lithospheric Seismic Project, Assumpção et al. (2002)). Station *capb* was a broad-band station operating in the frequency range 0.01 to 20 Hz. Stations *cap12* and *cap09* were short period stations operating in the 1–20 Hz band. MT soundings were collected in July 2003 with a commercial wide-band Metronix system recording three different frequency bands spanning a total frequency range from 2 mHz to 1 kHz.

2. Receiver functions

2.1. Definition

Receiver functions have been widely used in deep crustal and upper mantle studies. Here we show only a summary of the main concepts of the method. More complete reviews were given by Ammon et al. (1990), Ammon (1991) and Wilson and Aster (2003), for example. The recorded seismic waveform of a distant earthquake includes information about the source, path through the mantle and local structure under the station. The recorded traces Z (vertical component) and R (horizontal–radial component) of a P-wave train can be expressed in the frequency domain as:

$$Z(\omega) = S(\omega).E_Z(\omega).I(\omega)$$
$$R(\omega) = S(\omega).E_R(\omega).I(\omega) \quad (1)$$

Fig. 1. a) Location of the study region (square) and the three major cratonic basins (*AM* = Amazon, *PN* = Parnaíba, and *PR* = Paraná). Stars are the epicenters of the events used for the receiver functions. b) regional map with the boundaries of the Paraná Basin and the continental flood basalt (the two thick lines). Thin lines are iso-thicknesses (km) of the basalt layer based on the boreholes (dots). Gray lines show limits of the mains sedimentary sequences: *O* = Ordovician Rio Ivaí Supersequence, *D* = Devonian Paraná Supersequence, *CP*, *P* and *TR* = Gondwana-I Supersequence, *JK* = Botucatu Formation of the Gondwana-III Supersequence. c) Regional map with the boundaries of the Paraná Basin and the continental flood basalt (the two thick lines) with the isodepths contours of basement depth (thin lines, km) based on borehole information (dots). The rectangle indicates the study area shown in (d). d) Study area with seismic stations (solid triangles) and MT sites (crosses). Gray area is the thin cover of Bauru sediments (*Kb*), and white area is the Serra Geral basalt (*pKsg*).

where $S(\omega)$ is the source signature of the P-wave signal incident beneath the pack of layers near the station; $E_{Z,R}(\omega)$ are the response of the earth structure (i.e., the vertical/radial trace one would get at the surface for an incident pulse, $\delta(t)$, beneath the structure), and $I(\omega)$ is the instrument response. The Receiver Function, RF(t), is defined as the time-domain trace corresponding to the deconvolution:

$$\mathrm{RF}(\omega) = R(\omega) / Z(\omega) = E_R(\omega) / E_Z(\omega) \quad (2)$$

The deconvolution operation (dividing the radial by the vertical component) removes all effects from the earthquake source and propagation path in the mantle, contained in $S(\omega)$, making the receiver function dependent only on the structure beneath the station. Fig. 2 shows three different earthquakes recorded by station *capb* and their receiver functions. It can be seen that despite each earthquake having different signatures, their receiver functions are very similar, as expected.

For a steeply incident wave beneath a homogeneous, horizontally layered structure, all multiply reflected and conversions that arrive at the station as a P wave will have the vertical and horizontal components with the same amplitude ratio. For this reason, in the deconvolution process all smaller secondary P arrivals are cancelled and the only P-wave is the "direct" arrival (Ammon, 1991). In other words, multiple P-wave arrivals from reverberations within the structure cannot be distinguished easily from a source signature with several pulses, and so are removed in the deconvolution. Fig. 3 shows the three main converted phases expected from a single interface (bottom of layer 1) and the theoretical receiver function. The Ps conversion (labelled "1-s", where the first number refers to the interface) is followed by two multiply reflected phases (labelled here "1-2ps" and "1-p2s", according to the number of branches above the interface, i.e., two P-wave branches and one S-wave branch, or one P and two S branches, respectively). Note that only phases arriving at the station as S waves will show up in the receiver function, as all

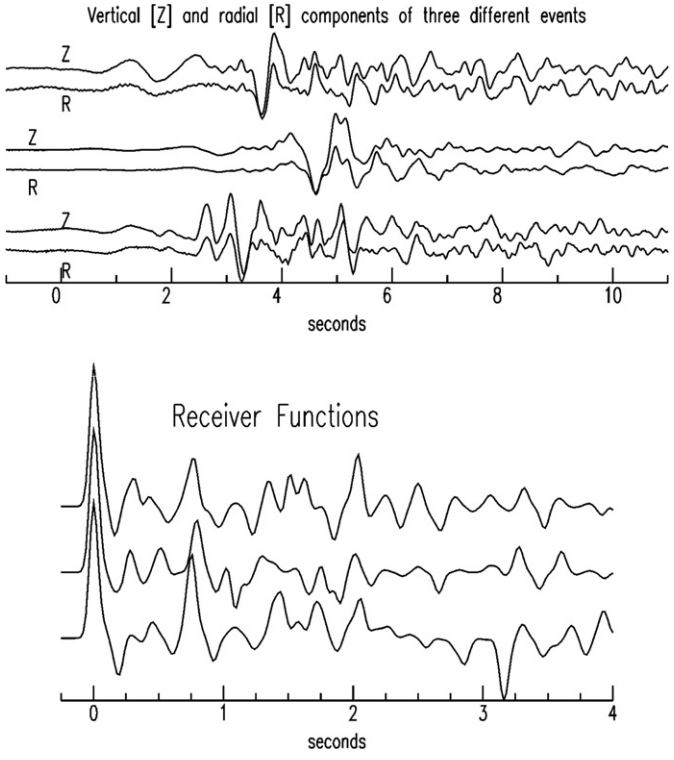

Fig. 2. Top) three different Andean earthquakes recorded at station *capb*; *Z* and *R* are the vertical and horizontal-radial components, respectively; first breaks are aligned at time zero. Bottom) receiver functions for each of the events showing similarity of the waveforms which depend only on the response of the structure beneath the station.

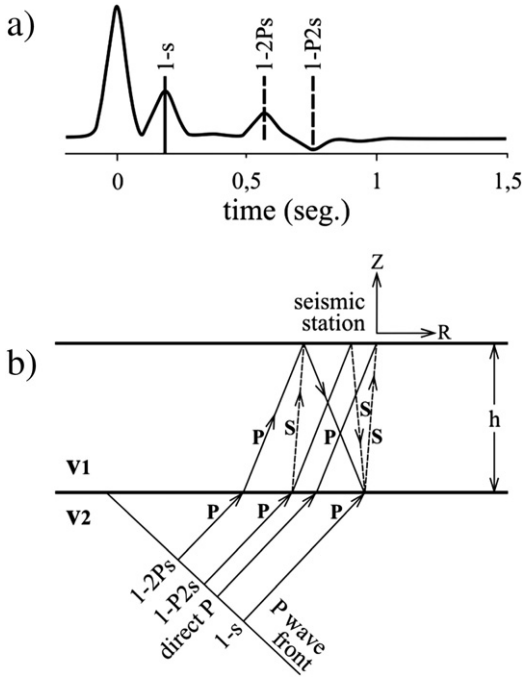

Fig. 3. Simplified diagram to show the various P-to-S converted waves from a single interface. a) Receiver function, b) ray-paths. Note that the phase 1-p2s is actually composed of two different phases with the same arrival time for horizontal layers: 1-pss + 1-sps.

other reverberations which arrive as P wave (such as 1-3p) will have the same radial/vertical amplitude ratio of the direct P wave and will not appear as independent later peaks in the receiver function (Ammon, 1991). So the receiver function trace, $RF(t)$, contains essentially all the P- to S-wave conversions, and reverberations at interfaces with velocity contrasts (e.g., Langston, 1979; Ammon et al., 1990; Ammon, 1991; Wilson and Aster, 2003).

Fig. 4 shows the expected receiver function from a sedimentary pack consisting of two (weathered and fresh) basalt layers overlying two sedimentary layers. Each interface, such as interface 2 (basalt/sediment) and interface 4 (sediment /basement) will produce three converted phases: one direct P-to-S conversion and two multiply reflected phases. Figs. 3 and 4 show that the multiply reflected phases have usually smaller amplitudes than the direct P-to-S conversions due mainly to inelastic attenuation. For values of Q_P and Q_S of 50 and 20, respectively, typical of shallow structures, the main peaks in a high-frequency receiver function are mainly due to direct P-to-S conversions. A velocity inversion, such as at the basalt/sandstone interface (bottom of layer 2 in Fig. 4) produces a P-to-S conversion with negative amplitude (peak 2-s).

2.2. Deconvolution methods

Several methods are available to deconvolve the vertical from the radial component. The most commonly used is simple spectral division of the radial and vertical FFT components, where Eq. (2) above is slightly changed to

$$\mathrm{RF}(\omega) = R(\omega).Z^*(\omega).G(\omega) / \left[Z(\omega).Z^*(\omega) + c(\omega)\right] \quad (3)$$

where $G(\omega)$ is a low-pass Gaussian filter to select the most useful frequency range of interest and $c(\omega)$ is a water level parameter to avoid division instabilities at spectral holes of the vertical component (Ammon et al., 1990).

The deconvolution can also be carried out in the time domain by iteratively constructing the receiver function trace with Gaussian

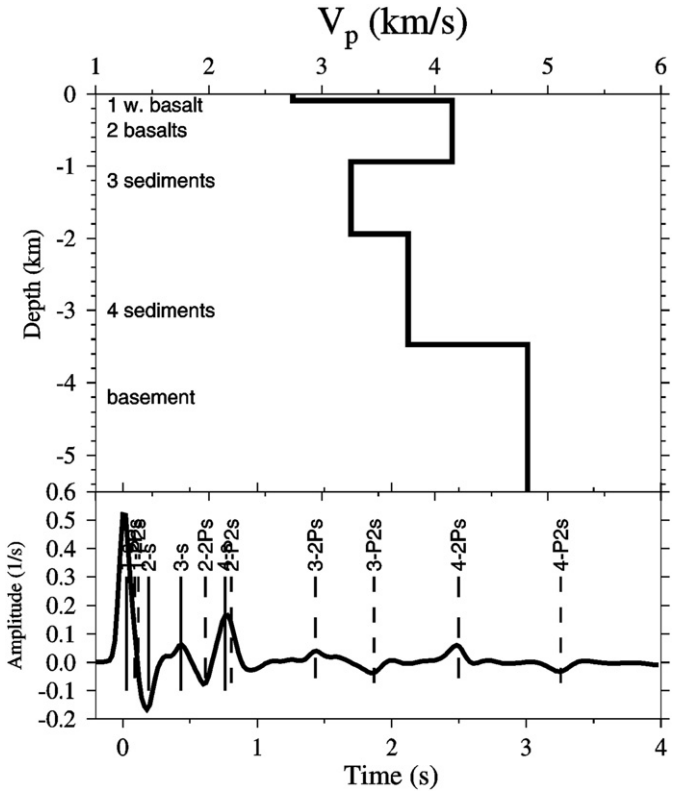

Fig. 4. Example of receiver function from a model of four layers over a half-space. Velocity model taken from the inversion results of station *capb*. The first number in the phase labels refers to the bottom of the layer at which conversion and reflections will occur. For example, "2-s" is the P-to-S conversion at the bottom of layer 2; phase "3-2ps" is the P incident at the bottom of layer 3, followed by two branches of P waves and one branch of S wave.

peaks such that its convolution with the vertical trace will best match the radial component (Ligorría and Ammon, 1999). The receiver functions in Fig. 2 were calculated with the time-domain method using a Gaussian filter corresponding to a 10 Hz low-pass filter.

A more robust frequency-domain deconvolution method was presented by Park and Levin (2000) using multiple taper spectral analysis (MTS) which minimizes spectral leakage, a common problem in short-length time series. The power spectra of each component is calculated as the average of several estimates using a series of orthogonal tapers, as shown in Eq. (4) below:

$$H_R(\omega) = \frac{\sum_{k=0}^{K-1} Y_R^k(\omega) \cdot \left(Y_Z^k(\omega)\right)^*}{\sum_{k=0}^{K-1} Y_Z^k(\omega) \cdot \left(Y_Z^k(\omega)\right)^* + S_0(\omega)} \quad (4)$$

where H_R is the receiver function, Y_Z is MTS estimation of the vertical component, Y_R is the MTS estimation of the radial component (for each taper k) and S_0 is the MTS estimation of the noise previous to the P wave arrival (used to stabilize the spectral division). K is the total number of used tapers, usually three or five.

2.3. Observed receiver functions

Modelling and inversion of receiver functions has been a powerful technique in the study of crustal and upper mantle discontinuities (e.g., Wilson and Aster, 2003). In studies of the deep crust, receiver functions are usually used for frequencies below about 1 Hz with a low-pass Gaussian filter commonly applied during the deconvolution process. This is due to the high frequencies being more susceptible to scattering from small scale lateral structure variations, as well as to the low strength of earthquake signals at frequencies above ~4 Hz when recorded at long teleseismic distances. For large-scale crustal studies, the near surface low-velocity layers in a sedimentary basin affect the shape of the receiver functions but are usually modelled as a single average layer (e.g., Assumpção et al., 2002; Meijde et al., 2003; An and Assumpção, 2004a,b). On the other hand, detailed information of the sedimentary layers, such as obtained by Julià et al. (2004), have rarely been a target for receiver functions analysis.

Here we used mainly intermediate depth Andean earthquakes because of their high frequency content, necessary to sample details within the sedimentary basin. Fig. 1a shows the epicenters of the two groups of earthquakes used in this study. The closer events, near the Chile–Argentina border at about 20° distance, range in magnitude from 4.6 to 6.0 m_b and have hypocentral depths from 50 to 190 km. The other group of events in Colombia, at a larger distance of about 40°, have magnitudes ranging from 5.3 to 6.6 and depths from 8 to 174 km, with the smaller events (m_b<5.5) being deeper than 100 km. The shape of the receiver function (i.e., the times and amplitudes of the Ps conversions and multiples) depends on the angle of incidence of the P-wave at the base of the receiver structure, which is determined by the slowness of the P arrival. The similar distances (and P-wave slownesses) within each earthquake group allows to stack the receiver functions to improve the signal-to-noise ratio.

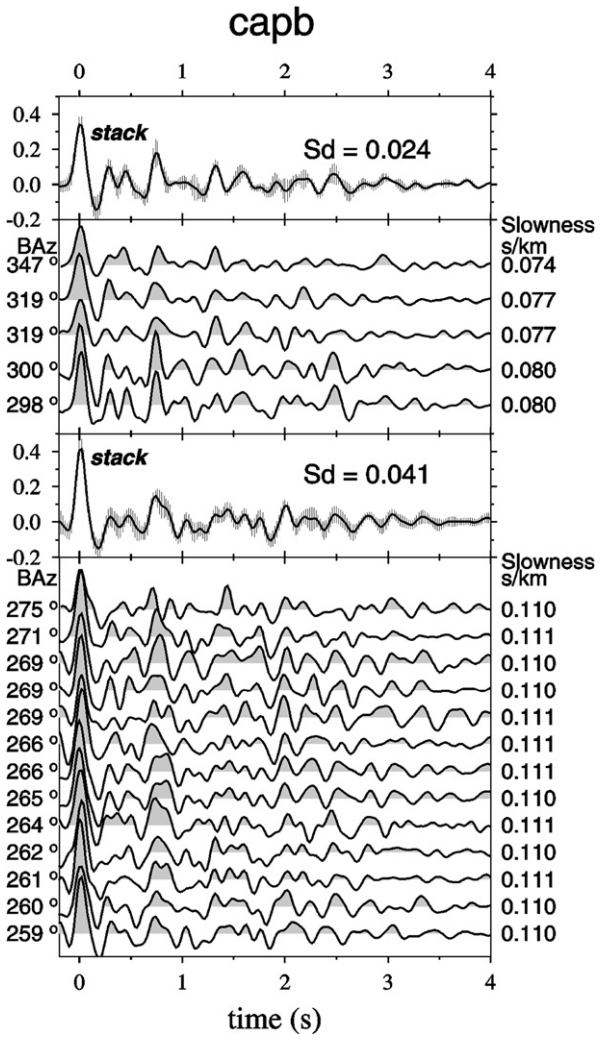

Fig. 5. Receiver functions for station *capb* calculated with the MTS deconvolution. Two groups of individual traces are shown, one for events from the West (bottom section, with slowness of 0.111 s/km), and the other for events from NW (top section, with slowness of 0.077 s/km). The weighted stack for each group (labelled "stack") was obtained using the pre-event *rms* noise as weights. Gray zone around the stacked trace denotes the standard deviation indicated as "Sd".

To obtain the receiver function of the sedimentary package, we used the first 20 s of the P-wave train, although only the first 3 s of the receiver functions were actually inverted. In the deconvolution we used both the time-domain and the multiple-taper methods, with frequencies up to 10 Hz. Several tests performed by Zevallos (2004) showed that the multiple-taper deconvolution gives slightly better results.

Fig. 5 shows the receiver functions of station *capb* from the two earthquake groups: Chile–Argentina border with back-azimuths to the West, and Colombia with back-azimuths to the NW. High coherence can be observed among the traces with one main peak at 0.75 s. The stacked traces were obtained by using the pre-event *rms* noise to weigh each individual trace. The stacked trace is shown with a gray band indicating the standard deviation of each stacked sample. The average of all standard deviations (denoted as "*Sd*" in Fig. 5) was later used in the inversion procedure. The stacked trace indicates there are at least two other smaller peaks at about 0.3 and 0.5 s. Fig. 6 compares the stacked traces for all three stations. Good coherence is observed among the three stations with two small peaks at about 0.3 and 0.5 s at all stations and a large peak (Ps conversion in the sediment/basement interface) at 0.75 s at *capb* and 0.9 s at the other two stations. This is a good indication that the structure of the sedimentary pack is relatively uniform beneath the three stations.

3. Magnetotelluric soundings

The magnetotelluric (MT) method uses measurements of naturally occurring electromagnetic fields to determine the resistivity of the sub-surface. The source signals are caused by magnetospheric and ionospheric currents (frequencies lower than 1 Hz) or by lightning discharges on a near global scale (frequencies higher than 1 Hz). The depth to which the incident electromagnetic fields penetrate depends on the frequency of the field and the resistivity of the medium. Thus, by studying the variation in response as a function of frequency, the variation in resistivity as a function of depth may be determined.

The fundamental quantity of interest for MT is the impedance tensor $\boldsymbol{Z}$ which is the transfer function between mutually orthogonal, horizontal components of the magnetic and electric fields,

$$\begin{aligned} E_x &= Z_{xx}H_x + Z_{xy}H_y \\ E_y &= Z_{yx}H_x + Z_{yy}H_y \end{aligned} \tag{5}$$

where E and H are the electric and magnetic fields, respectively, and (x,y) denote two orthogonal components in the horizontal direction.

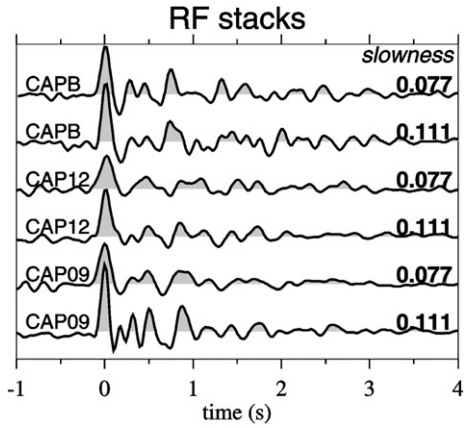

Fig. 6. Comparison of the RF stacks for the three stations. Numbers on the right are the average slowness of each stack. Note the large peak at 0.75 s for *capb* and 0.9 s for *cap12* and *cap09*, which is the P-to-S conversion at the sediment/basement interface.

For a one-dimensional (1D) horizontally-layered conductivity structure (as, for instance, in a sedimentary basin), the impedance tensor takes on a very simple form,

$$Z_{xy} = E_x / H_y = -Z_{yx} = -E_y / H_x; \qquad Z_{xx} = Z_{yy} = 0. \tag{6}$$

The MT response is commonly expressed through apparent resistivity and phase (scaled amplitude and phase of the impedance tensor components, respectively) and plots of these elements against frequency are the results of an MT sounding at a given site. A fuller description of the MT method is given by Vozoff (1991), for example.

In this study, MT data were collected at six different sites (Fig. 1d), one site near each of the seismic stations and three others more distant. All stations were processed in a single station mode, although twins were obtained with the same recording time. We used a coordinate system with one of the horizontal axis aligned with the magnetic meridian. The electric field variations were measured with 100 m dipoles, in a cross-configuration, with non-polarizable lead–lead chloride electrodes, whereas the magnetic fields were measured with induction coils for the two horizontal and one vertical components. The vertical magnetic field is sensitive to lateral resistivity contrasts and also provides a qualitative way of assessing the dimensionality of the data. As expected for a typical 1D environment, the vertical magnetic fields recorded at the MT sites of the Paraná Basin are near zero for periods with penetration within the sedimentary package.

The complex-valued MT tensor elements were estimated with the code of Egbert and Booker (1986). As the raw data had excellent quality, processing with remote reference was not necessary. Fig. 7 shows the apparent resistivity and phase curves for all sites after single station processing. The shape of the curves is typical of a sedimentary basin. The increase of the apparent resistivities up to about 0.1 s results from the increased resistivities of the fresh basalt layer. The low values between 1 and 10 s are caused by the low resistivities of the sedimentary layers, and the final increase at longer periods results from the high resistivities of the basement.

The similarity of apparent resistivities and phases calculated from the XY and YX components of the impedance tensor shows that the geoelectrical structure can be well explained with 1D models. This is consistent with the simple surface geology of the area (basalt outcrops and very shallow soil derived from basalt weathering) as seen in Fig. 1d. The geological variation seen in Fig. 1c (limit of sandstones/basalt) is relatively mild as the sediment thicknesses are very thin, not more than a few tens of meters. This limit, however, is probably responsible for the small static shift seen in site MT1 (Fig. 7), the only which departs from a purely 1D pattern.

Different tests of the impedance tensor confirmed the general 1D nature of the sedimentary pack. As an example, Fig. 8 shows plots of the rotated impedance tensor components Z_{xx} and Z_{xy} for site MT-4 at six different periods. These diagrams show that at short periods (with penetration into the sediments), the response is nearly 1D (off-diagonal Z_{xy} magnitudes circular, on-diagonals Z_{xx} nearly zero). At the two longest periods (with penetration into the crystalline basement), the response becomes more 2D with the orientation of the Z_{xy} magnitude in a NE–SW direction and the Z_{xx} nearly zero. Consequently, apparent resistivities and phases can be inverted to an assumed 1D layered structure up to the top of the basement under each site. Rotationally invariant data (Ranganayaki, 1984) have been used, as they proved useful in reducing the effects of local structures (Ingham, 1988).

4. Inversion of receiver functions

4.1. Linearized inversion

Modelling the receiver function waveform is a highly non-unique problem (e.g., Ammon et al., 1990) because any specific peak can be interpreted in different ways, such as a P to S conversion from a deep

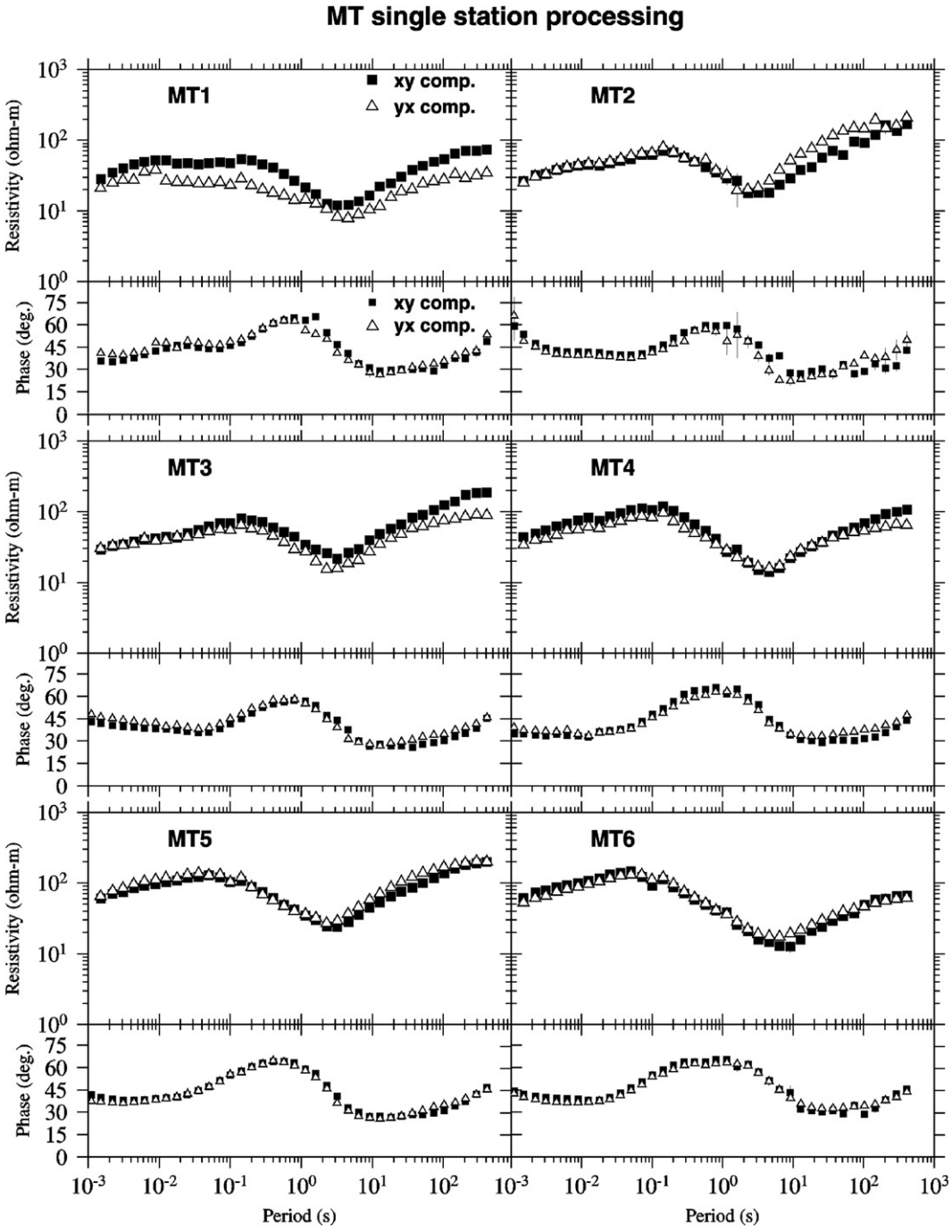

Fig. 7. Curves of apparent resistivities and phases for the six MT soundings.

interface or a multiply reflected phase from a shallower layer. Linearization methods can be used to model RF (Ammon et al., 1990) using several different starting models to account for the non-uniqueness. Regularization is often necessary, such as smoothness constraints, to stabilize the solutions. A test of a linearized inversion is shown in Fig. 9. We stacked 12 receiver functions for the West group (calculated by the time-domain deconvolution, as shown in Fig. 2). Because of the non-uniqueness problem the final solution depends strongly on the initial model. For this reason we used 24 different initial models, chosen randomly (Fig. 9a). Layer thicknesses were fixed

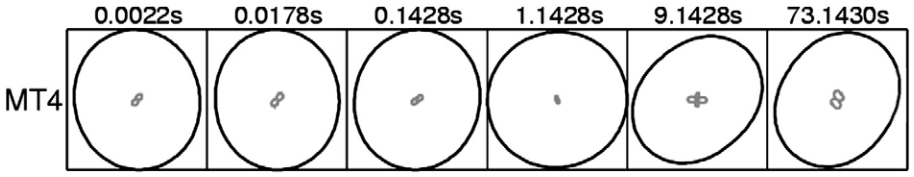

Fig. 8. Polar diagrams of impedance elements Z_{xx} (gray line) and Z_{xy} (black line) for site MT-4 at six different periods (given at the top of the corresponding ellipse).

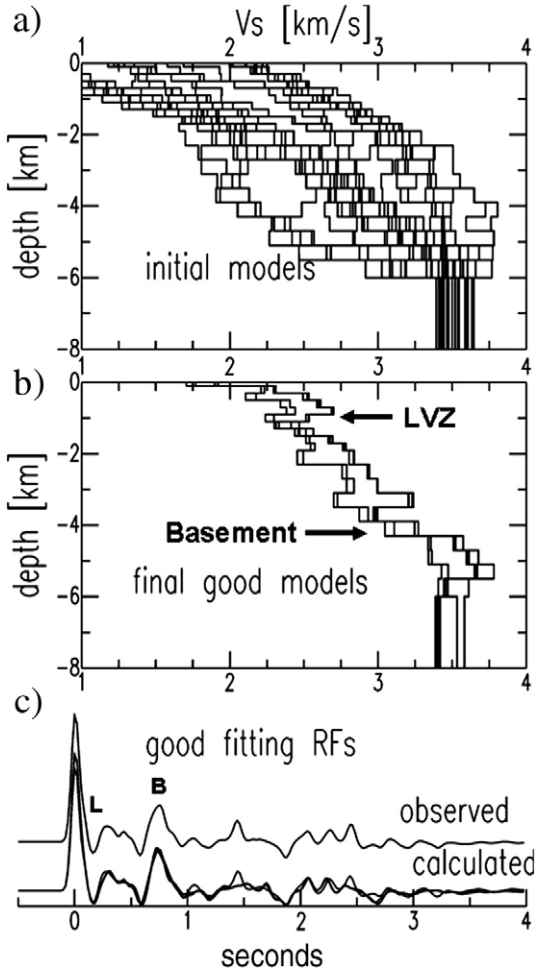

Fig. 9. Linearized inversion of the stacked receiver function (time-domain deconvolution) for station *capb*. a) S-wave velocity profiles for 24 different initial models. b) Best fitting resulting models showing a low-velocity zone starting near 1 km depth ("LVZ"), and a sudden velocity increase near 4 km depth ("Basement"). c) Observed and calculated RFs; "L" is the negative peak corresponding to the top of the low-velocity zone; "B" is the Ps conversion from the sediment/basement interface.

and S-wave velocities we iteratively inverted. *Vp*/*Vs* ratio was held constant at the standard 1.73 value. Only six runs converged to a good fitting model (Fig. 9b) while the remaining 18 inversions failed to provide a good fit to the observed receiver function, remaining in secondary minima of the solution space. Interestingly, despite the minor local differences in the velocity profile all six acceptable models have a common velocity inversion at about 1 km depth ("LVZ" in Fig. 9b) and a large velocity increase to about 3.5 km/s near 4 km depth. The shallow interface with a velocity inversion is the expected bottom of the basalt layer overlying sandstones and produces a negative peak in the receiver function (labelled "L" in Fig. 9c). The relatively sharp interface at the sediment/basement boundary is due to the large peak at 0.75 s in the receiver function (labelled "B" in Fig. 9c).

4.2. Inversion by genetic algorithm

Global search methods like Genetic Algorithm (e.g., Shibutani et al., 1996) or Neighbor Algorithm (e.g., Sambridge, 1999) can also be used to account for the solution diversity and non-linearity. Here we used a simple GA search to examine the possible range of the major structural features of the sedimentary basin: the high-velocity basaltic layer, the sedimentary sequence below the basalt, and basement depth.

For the direct problem, we calculated the receiver functions by first determining the seismic response of the layered structure (Kennett, 1983) and then deconvolving the radial by the vertical responses following the procedures of Ammon (1991). For the MT apparent resistivity and phase, we used the forward calculation of Constable et al. (1987).

Genetic Algorithm (GA) is a method to select the best models from a population of randomly chosen tentative models, based on "survival of the fittest" criteria (e.g., Holland, 1975; Whitley, 1994). The best models from one generation (population) are combined (mated) with cross-over operations to produce offspring models which will take part in a new, better fitting generation of models. The basis for using genetic mechanisms is that the cross-over operation has a good probability of combining the good genes (model parameters) from each parent and produce an offspring with a better fitting than any of its parents. Mutation operations, where one or more genes (model parameters) are randomly altered, are also important as they ensure population diversity and help avoid the population of models evolve towards a local minimum in fitting the data.

The parameters for the operations of selection, cross-over and mutation were set after test trials. We used a probabilistic binary tournament selection (the best fitting of two randomly chosen models is selected as a parent for the cross-over operation), a uniform cross-over with 94% probability, and a binary mutation probability of 6%. Each population has 120 models which evolve through 50 generations. The best model is passed to the next generation (called "elitism"). For each inversion, 50 different runs were carried out and the best final model in each run was saved, provided the misfit was lower than a predefined threshold based on the data uncertainty. After this process we have up to 50 acceptable models.

4.3. Parameter search ranges

GA is also useful for allowing the range of model parameters to be chosen according to a-priori geological information. We modelled the sedimentary basin as having four layers over a half-space: the first two layers represent weathered and fresh basalt, the third and fourth layers represent the main packs of sedimentary rocks, and the half-space is the granitic/gneissic basement. Table 1 shows the search range of all parameters for the 4-layer plus half-space model. *Vp*/*Vs* ratio was fixed for all layers at 1.76 based on analysis of local induced seismicity by Assumpção et al. (1995). Souza (1982) estimated *Vp*/*Vs* ratios of about 1.9 for the basalt and 1.7 for the underlying sediments, which would give an average value for the four layers close to the

Table 1
Parameter ranges used in the GA inversions.

Layer	*Vp* (km/s)	*Vs* (km/s)	*Vp*/*Vs*	Thickness (km)	Resistivity (Ωm)	Density (g/cm3)	Attenuation	
							Q_P	Q_S
1 — weathered basalt	3.17–3.87	1.8–2.2	1.76	0.02–0.3	10–100	2.40	50	20
2 — fresh basalt	3.87–5.46	2.2–3.1	1.76	0.15–1.0	40–1000	2.50	50	20
3 — sediment	2.99–4.05	1.7–2.3	1.76	0.2–2.0	2–300	2.45	50	20
4 — sediment	3.87–5.28	2.2–3.0	1.76	0.2–2.0	2–300	2.60	50	20
5 — basement	5.28–6.1	3.0–3.46	1.76	–	100–1000	2.75	100	50

Vp/*Vs* ratio, densities and *Q* were fixed.

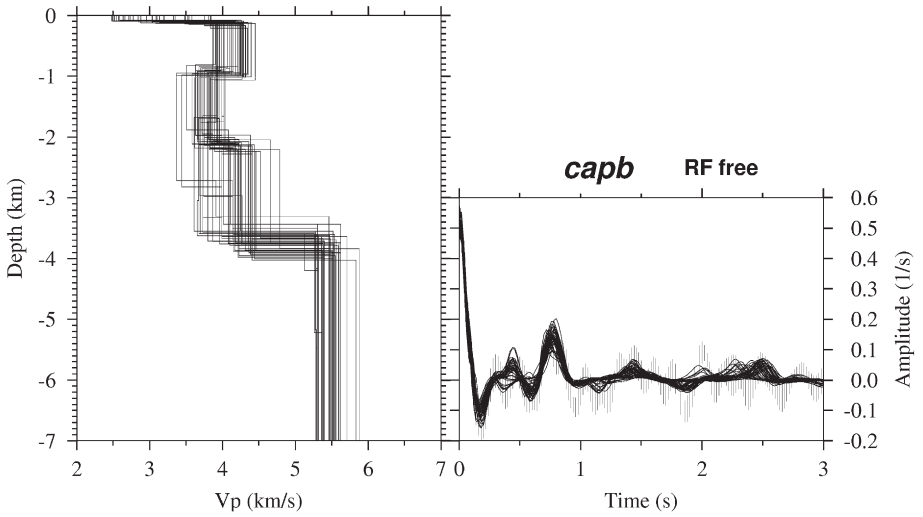

Fig. 10. Velocity models (left) inverted for station *capb*, using the stacked receiver function (MTS deconvolution) for slowness 0.111 s/km (right), after 50 GA runs. The displayed models have misfits less than the standard deviation of the observed stack (0.041 s^{-1}).

adopted 1.76. The limits for the P-wave velocity in the fresh basalt layer (about 3.9 to 5.5 km/s) were based on the ranges reported in seismic reflection work (Souza, 1982) and seismic refraction (Yamabe et al., 1997). MT soundings in the Paraná Basin (Stanley et al., 1985) show a range of resistivities from 2 Ωm near the surface to 500 Ωm in the basement. The density of each layer was fixed, based on Yamabe et al. (1997), Yamabe (1999) and well-logging data for the Paraná Basin (e.g., Milani et al., 1994). In the RF traces (Figs. 5 and 6) the amplitudes decrease after about 3 s due partly to inelastic attenuation in the sediments. We set the inelastic attenuation factors (Q_P and Q_S) in calculating the receiver functions as shown in Table 1.

Some additional geological constraints were imposed to the model. The seismic velocity of the sub-basalt layer should be smaller than the velocity of the fresh basalt, and the seismic velocity of the basement (half-space) must be larger than that of the overlying sedimentary layer. These geological constraints are met by the velocity ranges shown in Table 1. All parameters have upper and lower limits according to other regional studies of earth resistivity and seismic velocities in the Paraná Basin.

4.4. Inversion results

Here we only present inversions of the receiver function stack of the closest group of events, with slowness of 0.111 s/km, because the usually higher frequency content results in better resolution. Inclusion of the receiver functions of the other group (0.077 s/km) does not change the main results (Zevallos, 2004). To invert the receiver functions with GA, we define the misfit between observed (y_o) and calculated (y_c) receiver functions, with n samples, as the *rms* standard deviation Sd^t

$$Sd^t = \left[(1/n)\sum(y_o - y_c)^2\right]^{1/2} \tag{7}$$

For station *capb*, the *rms* standard deviation of the stacked trace for slowness 0.111 s/km (Fig. 5) is $Sd^o = 0.041\ s^{-1}$. In the GA inversion we defined the objective function to be minimized, F_{RF}, as

$$F_{RF} = \phi\left(Sd^t - Sd^o\right), \tag{8}$$

where $\phi = 0$, if $Sd^t < Sd^o$, or $\phi = 1$, if $Sd^t > Sd^o$. Thus, any model fitting the observed receiver function within its standard deviation is equally acceptable. This helps to keep model diversity in the final solution pool. Fig. 10 shows the resulting models after 50 GA runs with misfit less than 0.041 (i.e., $F_{RF} = 0$). Although a general trend can be recognized, the model diversity is large. Depth to basement lies in the range 3.3 to 4.0 km.

When we invert for the electrical structure using the MT data only, we minimize the combined standard deviations of the apparent resistivity and phase, defined as follows:

$$Sd_{MT} = \left[\left(\sum(\log\rho_o - \log\rho_c)^2 + \lambda\sum(\phi_o - \phi_c)^2\right)/2n\right]^{1/2} \tag{9}$$

where ρ and ϕ are the invariant resistivities and phases, respectively (data from Fig. 7), with n frequency components, and λ is a scaling factor of 1/500. The estimated standard deviation of the observed *log* (resistivities) is about 0.10 (taken from Fig. 7, for example) which corresponds to a mean error in the resistivities of 25%. The scale factor λ was chosen to make the phase deviation numerically similar to the resistivity deviation. Similarly to the RF inversion, the objective function to be minimized in the GA process was

$$F_{MT} = \phi(Sd_{MT} - 0.10), \tag{10}$$

where $\phi = 0$, if $Sd_{MT} < 0.10$, or $\phi = 1$, if $Sd_{MT} > 0.10$.

This means that any model fitting the MT data within the observed errors will be equally good in the GA search.

Fig. 11 shows the inversion of the magnetotelluric data for the MT-6 site, near station *capb*. In the MT inversion, besides the weathered

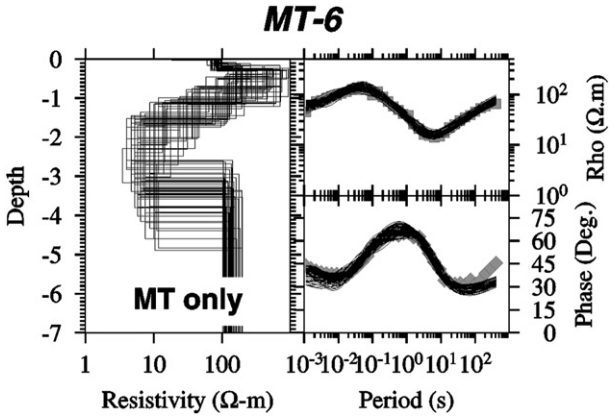

Fig. 11. Resistivity models (left) inverted for MT sounding number 6 (closest to station *capb*), after 50 GA runs. The displayed models have misfits less than the combined data variance of the observed data, i.e., $Sd_{MT} \leq 0.10$ (Eq. (9)).

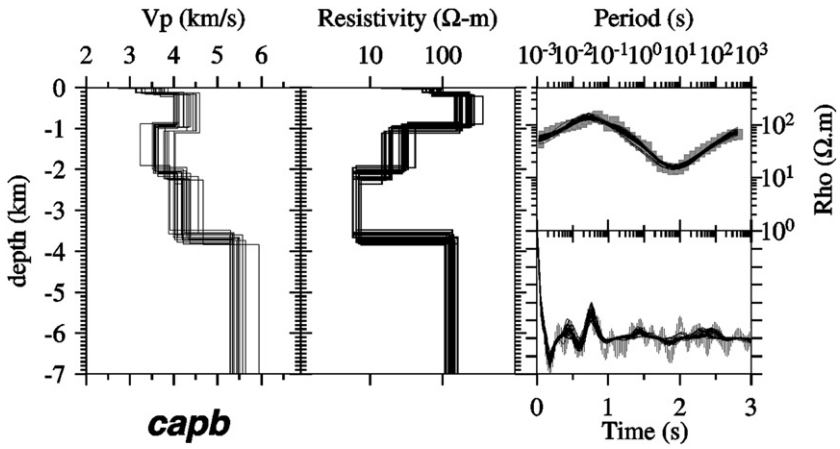

Fig. 12. Joint RF and MT inversion for station *capb*. Surviving models after 50 GA runs.

basalt layer, an additional thin surface layer representing the soil (fixed thickness of 10 m, not actually seen in Fig. 11) was found necessary to fit the MT data at very short periods. The resulting models from the MT inversion (with $F_{MT}=0$, Fig. 11) show the general trend of the resistivity profile with a large scatter in layer thicknesses and basement depth, typical of electromagnetic diffusion data.

5. Joint inversion with genetic algorithm

To overcome instability problems and reduce the space of possible solutions joint inversions of different types of data are being used more often, especially with electric and electromagnetic methods, such as MT and Schlumberger (VES) soundings (Vozoff and Jupp, 1975), CSEM and VES (Gomez-Trevino and Edwards, 1983), TEM and VES (Raiche et al., 1985). Different types of earth properties can also be used, such as joint inversion of geoelectric and surface wave seismic data (Hering et al., 1995), or VES and seismic refraction data (Gallardo and Meju, 2004). Joint inversion of RF and MT was used recently by Jones and Moorkamp (2006) in deep crustal and lithospheric studies.

In the joint inversion of receiver function and MT data, where the layer thicknesses are the common model parameters, we combine both misfit functions above (Eqs. (8) and (10)) but only use the apparent resistivities (MT phase data is not used in the joint inversion). The idea is to show that only a small contribution from the MT data is sufficient to reduce the ambiguities in the RF inversion. Besides, the phase is not a completely independent parameter from the modulus of the apparent resistivity as it is related to the variation of the modulus with frequency. Thus the objective function to be minimized in the joint inversion is

$$F_{\text{Joint}} = F_{\text{RF}} + \mu F_{\text{MT}} \tag{11}$$

where

$$F_{\text{MT}} = \phi(\text{Sd}_{\text{MT}} - 0.10), \text{ and } \quad \text{Sd}_{\text{MT}} = \left[(1/n)\sum(\log\rho_o - \log\rho_c)^2\right]^{1/2} \tag{12}$$

and μ is a scaling factor accounting for the different numerical values of each observation and also for the relative weight of each type of data in the joint inversion. Thus a value of $\mu=[0.041/0.10]/10$ was used. The results of the joint RF + MT inversion for station *capb* (Fig. 12) show better constrained velocity models (compared with RF-only inversion, Fig. 10). Not only the basement depth is better constrained (3.5–3.8 km range), but the transition between the upper and lower sedimentary sections is also better defined.

Although resistivity and seismic velocities are usually uncorrelated for any specific rock type, some empirical relationships encompassing widely different rock types (both sedimentary and igneous) have shown a slight trend of increasing velocities with increasing

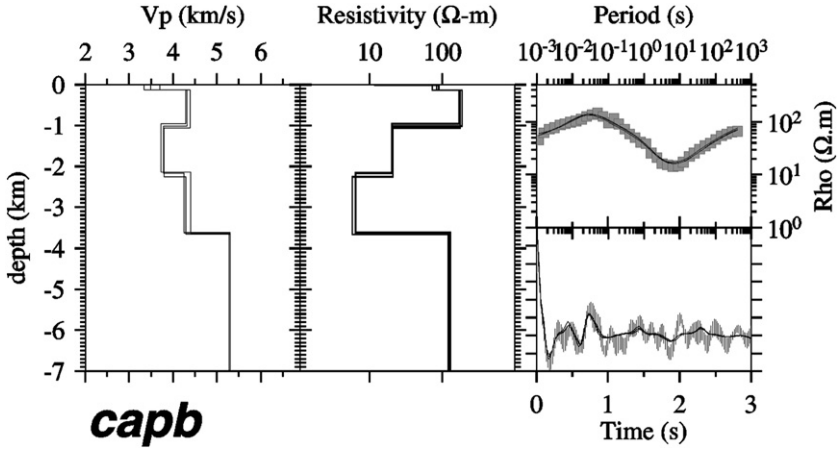

Fig. 13. Joint RF and MT inversion with flexible constraint from *Vp*×*rho* relationship. Surviving models after 50 GA runs. Only three models satisfy $F_{\text{Joint}}=0$.

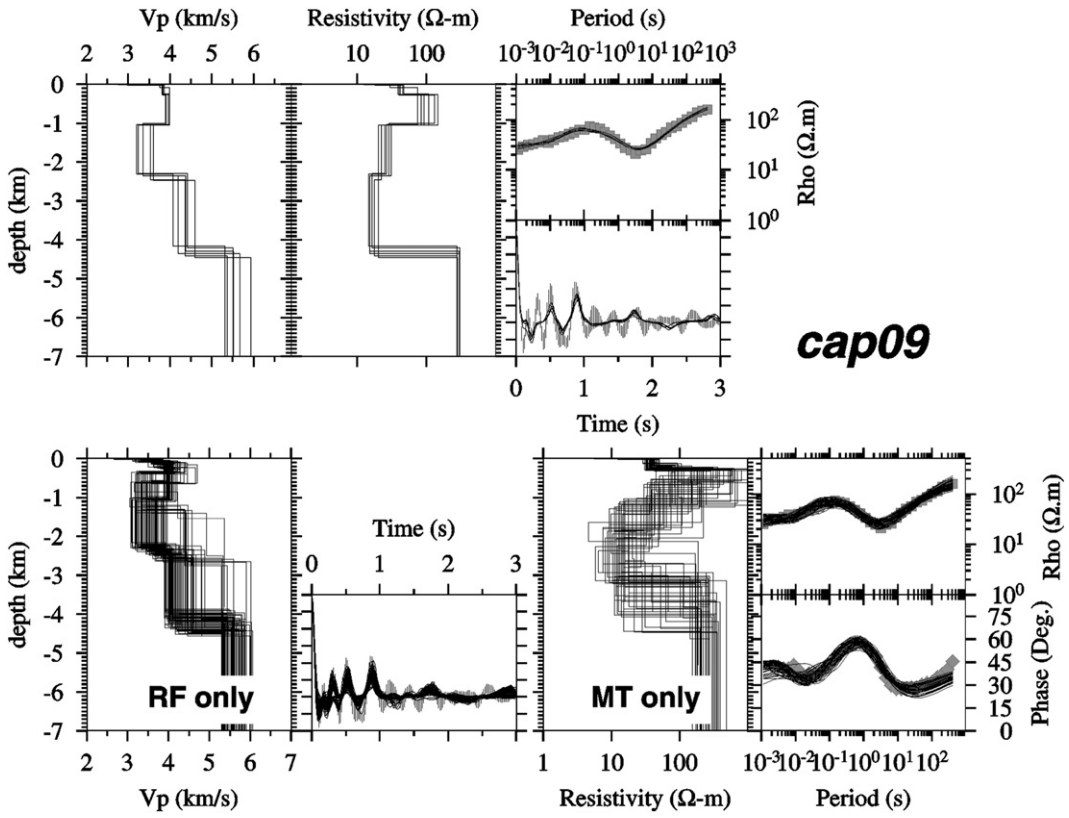

Fig. 14. Inversion results after 50 GA runs for station *cap09*. Inversion of Receiver Function only (bottom left), MT-3 sounding only (bottom right) and joint RF + MT with flexible constraints from *Vp* × *rho* relationship (upper figures).

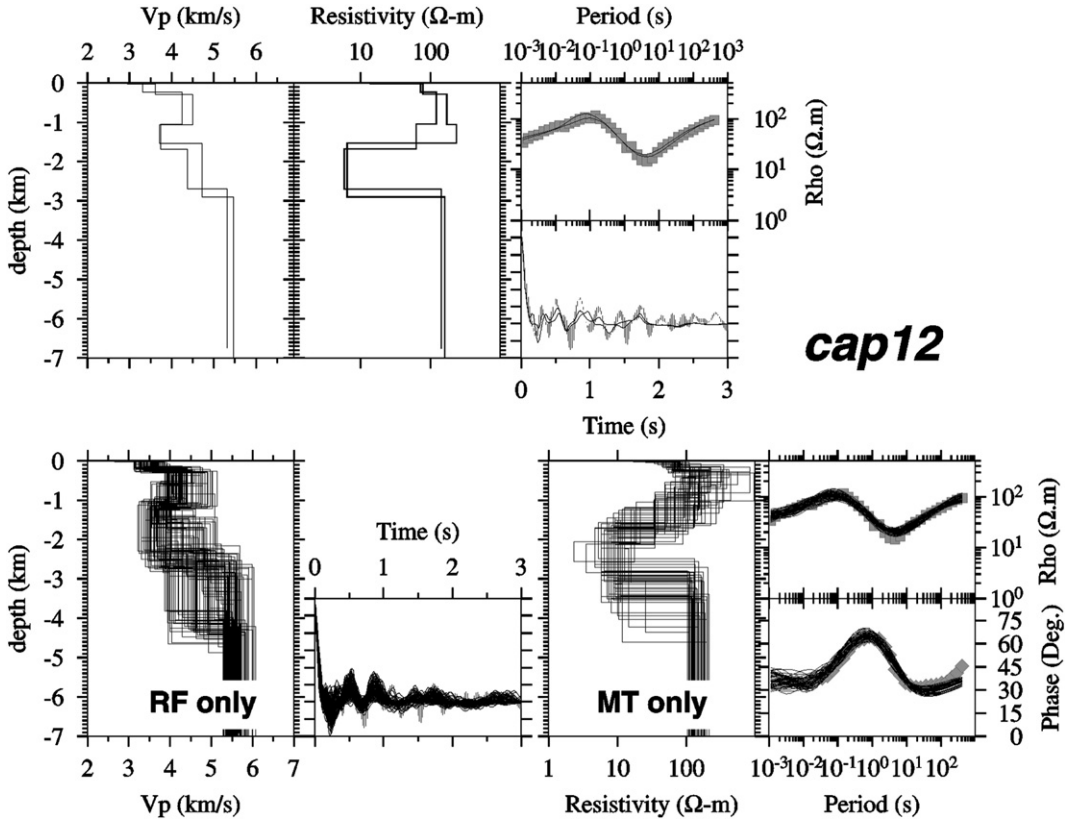

Fig. 15. Inversion results after 50 GA runs for station *cap12*. Inversion of Receiver Function only (bottom left), MT-4 sounding only (bottom right) and joint RF + MT with flexible constraints from *Vp* × *rho* relationship (upper figures).

resistivities. Dell´Aversana (2001) proposed the following empirical relationship, valid in the range $V_P = 3$ to 7 km/s and $\rho = 2$ to 20,000 Ωm:

$$V_P = 3.12 + 1.63\ ln(ln\,\rho);\ \text{km/s}. \quad (13)$$

We also tried this empirical relation $V_P \times \rho$ as an additional constraint in the joint inversion. Because of the large scatter in such empirical relationships we chose to use a penalty to the RF objective function, whenever the *average* difference between the *P* velocity of the model layer (V^m) and the velocity calculated from the layer's resistivity (V^r, using Eq. (13)) deviated more than 1 km/s. Thus, Eq. (8) was modified to

$$F_{RF} = \phi\left(Sd^t - Sd^o\right), \quad (14)$$

where

$\phi = 0$, if $Sd^t \le Sd^o$ and $\langle |V^m - V^r| \rangle$ less than 1 km/s
$\phi = 1$, if $Sd^t > Sd^o$ and $\langle |V^m - V^r| \rangle$ less than 1 km/s
$\phi = 2$, if $\langle |V^m - V^r| \rangle$ larger than 1 km/s.

We call this joint inversion as having a "flexible constraint" on V_P–ρ.

Fig. 13 shows the inversion results for station *capb* where only three models, out of all 50 GA runs, achieved a final objective function $F_{Joint} = 0$, i.e., satisfied all RF, MT and V_P–ρ constraints. Clearly, the solutions now are much better defined. The basalt layer and the half-space basement have relatively high velocities and high resistivities, compared with the sediments, as expected. However, the bottom sedimentary section has very low resistivity, despite having a seismic velocity higher than the upper section. This shows that including the penalties in Eq. (14) helps constrain the velocity models but still keeps resistivity and velocities as independent, useful information.

Data from the other stations, *cap09* and *cap12*, were processed in a similar way. Figs. 14 and 15 show the resulting models from the isolated RF and MT inversions as well as the joint inversion with flexible V_P–ρ constraints. Data from MT-3 sounding was used with station *cap09*, and MT-4 with station *cap12*. MT-1 sounding was not used with station *cap09* because of static shift (see Fig. 7) possibly caused by the nearby Bauru sediments. The isolated inversions ("RF-only" and "MT-only") show a general trend of a high velocity, high resistivity basalt layer, overlying a lower velocity and lower resistivity sedimentary pack. However, the joint inversion constrains the possible models much more effectively than the single inversions, as expected, defining the basalt thickness at 1.0 km and the basement depth at about 4.3 km (*cap09*) and 3.0 km (*cap12*).

6. Discussion

In deep crustal studies with low-frequency RFs, the correct identification of the Ps conversion (especially from the Moho discontinuity) is important to avoid non-uniqueness problems in the interpretation. This can be done with the variation of the move-out (time difference between the direct P and the converted Ps) as a function of incidence angle (or slowness), or by identifying the corresponding multiply reflected phases (Fig. 3). For very shallow interfaces, however, the move-out change with incidence angle is very small and not easily detected. For station *capb*, for example, the basement Ps conversion would have times of 0.75 and 0.72 s for slowness of 0.111 and 0.077 s/km, respectively, which is below our resolution. On the other hand, the higher attenuation (low *Q*) of shallow sedimentary rocks reduces the amplitudes of the multiples such that the strongest phases in the receiver function trace are most likely direct Ps conversions (Figs. 3 and 4). The consistent results obtained from both the linearized and the GA inversions (the negative trough close to the direct peak interpreted as the Ps from the base of the basalt layer, and the strong peak at ~0.75 s from the sediment/basement interface) support our interpretation of the strong Ps conversion from the upper crustal basement. Similar results were obtained by An and Assumpção (2004b) and Costa et al. (2006) with other stations in the Paraná Basin where the largest peak in the RF trace yielded basement depths in agreement with data from nearby deep wells.

The improved resolution of the joint RF + MT inverted models is best illustrated by station *capb* (Figs. 10–12). The basement depth defined in the range 3.3 to 4.0 km (RF only) and 2.6 to 4.8 km (MT only) was more sharply defined at 3.5 to 3.8 km in the joint inversion (Fig. 12). Including MT data decreased the range of basement depths to half the value for the isolated RF models. A slight improvement of the bottom of the basalt layer was also observed, from 0.8–1.1 km (RF only) to 0.9–1.1 km (joint inversion). In this case the contribution of the MT data was less significant probably because of its poor resolution for this interface, as seen in Fig. 11. The use of empirical relations between resistivity and seismic velociy (Eqs. (13) and (14)), even with a small influence, proved very useful in further constraining the solutions.

The three joint RF + MT inversions (Figs. 13–15) show that some features are consistently observed at all stations: a shallow surface layer, about 100–200 m thick, with low velocity and low resistivity (altered basalt). Below, the fresh basalt layer is seen as a high velocity and high resistivity layer. The total basalt thickness is well defined at about 1.0 km for all three stations. The velocity inversion zone, seen at about 1 km depth, coincides with a low resistivity zone (except for station *cap12*) corresponding to the sedimentary pack. The high-velocity half-space has high resistivity confirming it is the crystalline basement. The results for the basement depth at stations *cap09* and *capb* are similar (3.8 and 4.3 km) and consistent with the expected depths based on regional well data (Fig. 1c). Considering that these two stations are about 20 km apart, this difference of 0.5 km does not violate our 1D assumption in the inversion for each station.

The basement depth obtained at station *cap12* (about 3.0 km) seems too shallow and two possible causes of error can be pointed out: 1) the Ps conversion from the basement is very weak, as shown in Fig. 6, which makes the basement depth harder to constrain; and 2) the direct P wave (first peak in Fig. 6) has lower amplitude than expected for that epicentral distance and slowness. This low amplitude could not be modelled adequately in the inversion (Zevallos, 2004) and is probably an indication of lateral variation beneath the station. (For the other two stations the first peak has larger amplitude and is well fit by the inverted models). Because of the poorer quality of the receiver functions, the results for station *cap12* are less reliable than *capb* and *cap09*. In addition, our simple GA algorithm may not have succeeded in interpreting the correct Ps conversion from the basement (at 0.85 s in Fig. 6) in the joint inversion and fitted the peak at 0.5 s as the basement Ps instead. Possible solutions to this problem would be the use of more layers (and possibly smoothness constraints) and more competent GA algorithms, such as Bayesian optimization (e.g., An and Assumpção, 2004a).

Interestingly, all joint inversions show a much lower resistivity in the deeper sedimentary section, despite the seismic velocity being higher than the upper sedimentary section. This feature, observed even in the less reliable station *cap12*, indicates different rock properties within the sedimentary pack.

7. Conclusions

High frequency (up to ~10 Hz) teleseismic receiver functions contain important information on the seismic velocities of sedimentary basins but, in general, have not been used in studies of upper crustal structure. In the case of the Paraná intracratonic basin, very good consistency was obtained for receiver functions from different earthquakes, probably due to the predominance of flat-lying strata beneath most of our study area. MT sounding helped reduce

ambiguities and non-uniquenesses common to the RF inversion and improved the resolution of the final acceptable models. Intermediate depth earthquakes from the nearby Nazca subduction zones are a good source of high-frequency P waves. This makes RF + MT joint inversion a promising tool to investigate basement depth and the major structural properties of intracratonic basins in Brazil, especially in areas where 1D models can be a good approximation.

Acknowledgements

Work supported by FAPESP grants 00/00806-5 and 01/06066-6, CNPq grant 30.4809/03-9 and CAPES PhD scholarship. We thank Luis Carlos Ribotta (IPT-São Paulo) for field work and general support during installation and operation of the seismic stations. We thank the editor and reviewers for valuable suggestions to improve the paper.

References

Ammon, C., 1991. The isolation of receiver effects from teleseismic P waveforms. Bull. Seism. Soc. Am. 81, 2504–2510.
Ammon, C., Randall, G., Zandt, G., 1990. On the nonuniqueness of receiver function inversions. J. Geophys. Res. 95, 15303–15318.
An, M., Assumpção, M., 2004a. Multi-objective inversion of surface waves and receiver functions by competent genetic algorithm applied to the crustal structure of the Paraná Basin, SE Brazil. Geophys. Res. Lett. vol. 31 (5), L05615. doi:10.1029/2003GL019179.
An, M., Assumpção, M., 2004b. Basement depth in the Paraná Basin with high frequency receiver functions. I Regional Geophysical Symposium Braz. Geophysics Soc., São Paulo, extended abstract, Brazilian Geophysics Society (SBGf), Rio de Janeiro, Brazil.
Assumpção, M., Freire, M., Ribotta, L.C., 1995. Sismicidade induzida no reservatório de Capivara: resultados preliminares sobre localização de fraturas ativas. IV Int. Congr. Braz. Geophys. Soc., Rio de Janeiro, Brazilian Geophysics Society (SBGf), Rio de Janeiro, Brazil.
Assumpção, M., James, D., Snoke, A., 2002. Crustal thicknesses in SE Brazilian shield by receiver function analysis: implications for isostatic compensation. J. Geophys. Res. 107 (B1). doi:10.1029/2001JB000422.
Constable, S.C., Parker, R.L., Constable, C.G., 1987. Occam's inversion: a practical algorithm for generating smooth models from EM sounding data. Geophysics 52, 289–300.
Costa, T.N., Assumpção, M., Barbosa, J.R., 2006. Estudo de espessura sedimentar na Bacia do Paraná com funcão do receptor de alta freqüência. II Regional Geophysical Symposium Braz. Geophysics Soc., Natal, extended abstract, Brazilian Geophysics Society (SBGf), Rio de Janeiro, Brazil.
Dell´Aversana, P., 2001. Integration of seismic, MT and gravity data in a thrust belt interpretation. First Break 19.6, 335–341.
Egbert, G.D., Booker, J.R., 1986. Robust estimation of geomagnetic transfer functions. Geophys. J. R. astr. Soc. 87, 173–194.
França, G., Assumpção, M., 2003. Estrutura da crosta em Goiás, usando a função do receptor, e mapa preliminar de espessuras crustais no SE e centro-oeste do Brasil. 8th Int. Congr. Braz. Geophys. Soc., Rio de Janeiro, Brazilian Geophysics Society (SBGf), Rio de Janeiro, Brazil.
Gallardo, L.A., Meju, M.A., 2004. Joint two-dimensional DC resistivity and seismic travel time inversion with cross-gradient constraints. J. Geophys. Res. 109. doi:10.1029/2003JB002716.
Gomez-Trevino, E., Edwards, R.N., 1983. Electromagnetic soundings in the sedimentary basin of Southern Ontario — a case history. Geophysics 48, 311–326.
Hering, A., Misiek, R., Gyulai, A., Ormos, T., Dobroka, M., Dresen, L., 1995. A joint inversion algorithm to process geoelectric and surface wave seismic data, part I: basic ideas. Geophysical Prospecting 43, 135–156.
Holland, J., 1975. Adaptation in natural and artificial systems. The University of Michigan Press, Ann Arbor.
Ingham, M.R., 1988. The use of invariant impedances in magnetotelluric interpretation. Geophys. J., Oxford 92 (1), 165–169.
Jarchow, C., Catchings, R., Lutter, W., 1994. Large explosive source, wide-recording aperture, seismic profiling on the Columbia Plateau, Washington. Geophysics 59, 259–271.
Jones, A.G., Moorkamp, M., 2006. Are seismic velocities and electrical conductivities reconcilable? AGU Fall Meeting, Abstracts, American Geophysical Union, Washington, USA.
Julià, J., Herrmann, R., Ammon, C., Akinci, A., 2004. Evaluation of deep sediment velocity structure in the New Madrid zone. Bull. Seism. Soc. Am. 94, 334–340.
Kennett, B.L.N., 1983. Seismic wave propagation in stratified media. Cambridge, UK. 342 pp.
Langston, C.A., 1979. Structure under Mount Rainier, Washington, inferred from teleseismic body waves. J. Geophys. Res. 85, 4749–4762.
Ligorría, J.P., Ammon, C., 1999. Iterative deconvolution and receiver–function estimation. Bull. Seism. Soc. Am. 89, 1395–1400.
Milani, E.J., 2004. Comentários sobre a origem e evolução tectônica da Bacia do Paraná. In: Mantesso-Neto, V., et al. (Ed.), Geologia do Continente Sul-Americano: Evolução da Obra de Fernando Flávio Marques de Almeida, Beca Editora, São Paulo, Brazil, pp. 265–279.
Milani, E.J., Ramos, V.A., 1998. Orogenias Paleozóicas no domínio sul-ocidental do Gondwana e os ciclos de subsidência da Bacia do Paraná. Rev. Bras. Geoc. 28, 473–484.
Milani, E.J., França, A., Schneider, R., 1994. Bacia do Paraná. Boletim de Geociências daPetrobrás 8 (1), 69–82.
Meijde, M., Van der Lee, S., Giardini, D., 2003. Crustal structure beneath broad-band seismic stations in the Mediterranean region. Geophys. J. Int. 152, 729–739.
Moritz, M.F., White, R.S., 2001. Seismic structure of basalt flows from surface seismic data, borehole measurements, and synthetic seismogram modelling. Geophysics 66 (6), 1925–1936.
Owens, T.J., Zandt, G., Taylor, S.R., 1984. Seismic evidence for an ancient rift beneath the Cumberland Plateau, Tennessee. a detailed analysis of broadband teleseismic P waveforms. J. Geophys. Res. 89 (B9), 7783–7795.
Park, J., Levin, V., 2000. Receiver functions from multiple-taper spectral correlation estimates. Bull. Seism. Soc. Am. 90, 1507–1520.
Raiche, A.P., Jupp, D.L.B., Rutter, H., Vozoff, K., 1985. The joint use of coincident loop transient electromagnetic and Schlumberger sounding to resolve layered structures. Geophysics 50, 1618–1627.
Ranganayaki, R.P., 1984. An interpretive analysis of magnetotelluric data. Geophysics 49, 1730–1748.
Rosa, A., Tassini, J., Backus, M., 1982. Seismic data quality in a basalt covered basin. 62th SEG meeting, expanded abstracts, Society of Exploration Geophysicists (SEG), Tulsa, USA, S5.5.
Sambridge, M., 1999. Geophysical inversion with a neighbourhood algorithm - I, Searching a parameter space. Geophys. J. Int. 138, 479–494.
Shibutani, T., Sambridge, M., Kennett, B., 1996. Genetic algorithm inversion for receiver functions with application to crust and uppermost mantle structure beneath Eastern Australia. Geophys. Res. Lett. 23, 1829–1832.
Souza, J., 1982. Transmission of seismic energy through the Brazilian Paraná Basin layered basalt stack. 62th SEG meeting, expanded abstracts, Society of Exploration Geophysicists (SEG), Tulsa, USA, S5.6.
Stanley, W., Saad, A.R., Ohofugi, W., 1985. Regional magnetotelluric surveys in hydrocarbon exploration, Paraná Basin, Brazil. Am. Ass. Petroleum Geol. Bull. 69, 346–360.
Vozoff, K., 1991. The magnetotelluric method. In: Nabighian, E. (Ed.), Electromagnetic methods in Applied Geophysics. Society of Exploration Geophysics, Tulsa, pp. 641–711.
Vozoff, K., Jupp, D.L.B., 1975. Joint inversion of geophysical data. Geophys. J. R. astr. Soc. 42, 977–991.
Yamabe, T.H., 1999. Estudos geofísicos para explicar a sismicidade induzida e orientar a exploração de água subterrânea em Nuporanga - SP; *PhD thesis (in Portuguese)*, IAG-USP, São Paulo.
Yamabe, T.H., Berrocal, J., Diogo, L.A., 1997. Seismic surveys in the northeastern portion of the Paraná Basin. 5th Int. Congr. Braz. Geophys. Soc., CD-ROM, Brazilian Geophysics Society (SBGf), Rio de Janeiro, Brazil.
Wilson, D., Aster, R., 2003. Imaging crust and upper mantle seismic structure in the southwestern United States using teleseismic receiver functions. The Leading Edge 22 (3), 232–237.
Whitley, D., 1994. A genetic algorithm tutorial. Colorado State University. http://samizdat.mines.edu/ga_tutorial.
Zandt, G., Ammon, C., 1995. Continental crust composition constrained by measurements of crustal Poisson´s ratio. Nature 374, 152–154 (9 March 1995).
Ziolkowski, A., Fokkema, J.T., 1986. The progressive attenuation of high-frequency energy in seismic-reflection data. Geophys. Prospect. 34 (7), 981–1001.
Ziolkowski, A., Hanssenn, P., Gatliff, R., Jakubowicz, H., Dobson, A., Hampson, G., Li, X., Liu, E., 2003. Use of low frequencies for sub-basalt imaging. Geophys. Prospect. 51, 169–182.
Zevallos, I., 2004. Modeling the Paraná basin, Capivara reservoir, through joint inversion of receiver function and magnetotelluric sounding. *PhD thesis (in Portuguese)*, University of São Paulo, Brazil, 101pp.